Laser-induced ultrafast spin current pulses: A thermodynamic approach

Laser-induced ultrafast spin current pulses: a thermodynamic approach

OPEN ACCESS
IOP Publishing
Journal of Physics: Condensed Matter
J. Phys.: Condens. Matter **29** (2017) 214002 (6pp)
https://doi.org/10.1088/1361-648X/aa6a76

Laser-induced ultrafast spin current pulses: a thermodynamic approach

A Fognini[1], T U Michlmayr[2], A Vaterlaus[2] and Y Acremann[2]

[1] Kavli Institute of Nanoscience Delft, Delft University of Technology, Delft 2628 CJ, The Netherlands
[2] Laboratory for Solid State Physics, ETH Zurich, 8093 Zurich, Switzerland

E-mail: acremann@solid.phys.ethz.ch

Received 16 January 2017, revised 28 March 2017
Accepted for publication 31 March 2017
Published 24 April 2017

Abstract

The ultrafast demagnetization process allows for the generation of femtosecond spin current pulses. Here, we present a thermodynamic model of the spin current generation process, based on the chemical potential gradients as the driving force for the spin current. We demonstrate that the laser-induced spin current can be estimated by an easy to understand diffusion model.

Keywords: ultrafast transport, spin dynamics, spin injection, spintronics

(Some figures may appear in colour only in the online journal)

1. Introduction

The models describing laser-driven ultrafast demagnetization [1] can be separated into two groups. The first approach is based on spin flips taking place in the bulk of the ferromagnetic material [2–13] where in particular Mueller *et al* [14] identified the chemical potentials for minority and majority electrons as the driving force for spin flips. The second approach describes the demagnetization as a transport effect, where a spin current transports the angular momentum away from the sample surface. There, spin flips can take place outside the view of the observer [15]. The proposed spin current has been experimentally observed by several groups [16–21], offering the opportunity to generate femtosecond spin current pulses. Kimling *et al* [22] developed a model of laser driven spin currents generated by the spin-Seebeck effect.

Spin currents play an important role in the demagnetization dynamics. In figure 1, we collected measured demagnetization times from the literature. The demagnetization times are plotted as a function of the resistivity of the materials investigated. There is a correlation between the demagnetization time τ and the resistivity ρ: materials with a higher resistivity tend to demagnetize on a longer time scale than good metals.

In this paper, we discuss the generation of femtosecond spin currents in the framework of diffusive transport. We discuss the concepts of spin currents in the field of spintronics and the possible implications of extending spin transport to the femtosecond time scale. Our approach is a simplification and approximation of the super-diffusive transport model by Battiato *et al* [15], aimed at giving an intuitive picture of the spin current generation process. It relies solely on three material specific input parameters: the spin resolved density of states, the absorption length, and the macroscopic resistivity.

2. Diffusive spin transport and the two current model

If we define our quantization axis along the magnetization direction of our ferromagnet, the electrons can be separated into a population of minority (↓)- and majority (↑) electrons [24]. In a diffusive description, we can assign an electrochemical potential to each of the two populations $\mu_\downarrow$, $\mu_\uparrow$. A gradient in the electrochemical potentials causes a current density for the minority- and majority electrons, which are denoted as $j_\downarrow$, $j_\uparrow$. Using these quantities, we can define a *charge current density* $j_c = j_\uparrow + j_\downarrow$, and a *spin current density* $j_s = j_\uparrow - j_\downarrow$. Due to charge neutrality in a metal, the charge current density is free of sources: $\nabla \cdot \vec{j}_c = 0$. However, spin flips can cause a coupling between the minority- and majority population. This implies, that the spin current can be lost along the path of transport, and therefore $\nabla \cdot \vec{j}_s \neq 0$.

A spin polarized current can be generated by passing a charge current across the interface between a ferromagnet and

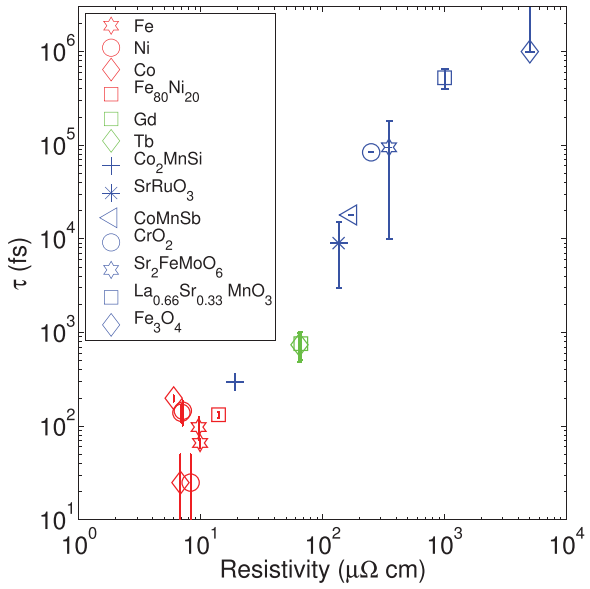

Figure 1. Demagnetization time from literature data, see table 1, plotted as a function of the resistivity. A higher resistivity goes along with a longer demagnetization time. The colors indicate different material classes: transition ferromagnets (red), lantanides (green), and half metals (blue). Reproduced with permission from [23].

a copper layer. Due to the different conductivities of the two spin species within the ferromagnet, we will obtain a difference $\mu_s = \mu_\uparrow - \mu_\downarrow$ near the interface (within the ferromagnet as well as the copper layer). This spin imbalance can be translated into a *spin voltage* $V_s = \frac{1}{q}(\mu_\uparrow - \mu_\downarrow)$ with q being the elementary charge. It causes an accumulation of spins at the interface and a difference between $j_\uparrow$ and $j_\downarrow$, causing spin transport along the charge current flow. A special case of a spin polarized current is the *pure spin current*: here, $j_s \neq 0$ while $j_c = 0$. The first time a pure spin current has been observed was by Jedema *et al* [25] in a non-local transport experiment. Pure spin currents can also be generated by the spin-Hall effect [26].

On the application side, the generation and detection of spin currents led to the discovery of the giant magnetoresistance effect [27–29], which led to a major improvement of hard disk read heads. Large spin currents can be injected into a ferromagnet. In this case, it is even possible to switch magnetic nano-structures by spin-injection [30]. It has been observed, that the effective damping of spin waves can be altered by spin-injection [31], leading to steady state precession. This may have applications for nanometer scale, tunable microwave oscillators. These findings and the discovery of the spin-orbit torque led to a better understanding of spin transport and may lead to novel non-volatile memory devices based on magnetic nanostructures.

3. Thermalization of the electron gas on the femtosecond time scale

We assume, that the electron gas is in a thermalized state immediately after the laser pulse. This is required in order treat the occupation of states by the Fermi–Dirac function.

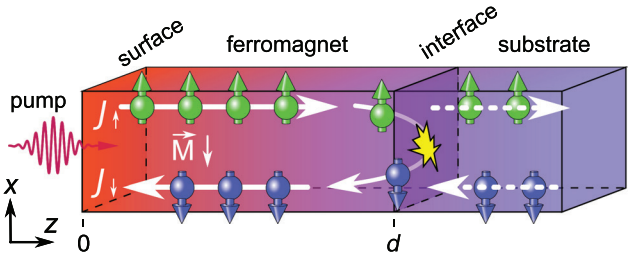

Figure 2. Schematic representation of the model: the pump laser pulse generates a temperature gradient within the ferromagnet causing a strong spin-current away from the surface. Spin angular momentum can either be dumped into the substrate or flipped at the interface. The initial magnetization of the sample points along the negative x-direction. Reproduced with permission from [23].

This approximation is not necessarily justified, as non-thermal hot electron distributions have been observed experimentally. Rhie *et al* [32] measured the occupation near the Fermi energy by time resolved photoelectron spectroscopy on Ni. They report a distribution, which deviates from the Fermi–Dirac function even 400 fs after the pump laser pulse. In order to estimate the influence of the non-thermal electrons on our transport model, we determine the number of non-thermal electrons from their experiment. The main result is shown in figure 2 of their publication [32]. In the following, the subscripts indicate the curves **a** to **d** form their figure 2. The measured photoemission intensity $I_b(E)$ for the pump-probe delay $t_b = 0$ fs shows clear signs of non-thermal electrons for energies $E > 0.5$ eV. At $t_c = 200$ fs the electron gas is almost completely thermalized, while the temperature (given by the slope for $E < 0.5$ eV) remains unchanged. Therefore, the measurements at $t_b = 0$ fs and $t_c = 200$ fs give us the opportunity to estimate the contribution of non-thermal electrons n_{nt} as

$$n_{nt} = \int_{E_f+0.5\,eV}^{E_f+2.0\,eV} I_b(E) - I_c(E)dE. \quad (1)$$

For comparison, we estimate the number of electrons above the Fermi energy, which have been excited by the laser pulse as

$$n_{ex} = \int_{\mu_b}^{E_f+2.0\,eV} I_b(E)dE - \int_{\mu_a}^{E_f+2.0\,eV} I_a(E)dE. \quad (2)$$

Here, $I(t_a)$ is the intensity measured for a negative pump-probe delay, corresponding to the state at room temperature and $\mu_{a,c}$ are the chemical potentials determined by fitting a Fermi–Dirac function to their data. The ratio n_{nt}/n_{ex} is ≈8%. Based on this small number, we approximate the electron gas as being thermalized immediately after the laser pulse.

4. Thermally induced spin current

In the following, we discuss the generation of a spin current pulse driven by an ultrafast optical excitation of a ferromagnet. Figure 2 shows the section of a ferromagnetic thin film of thickness d deposited on a substrate. The demagnetization process is initiated by the absorption of a 800 nm intense ultrafast laser pulse, which is linearly polarized and at normal incidence to the sample surface. Such a pulse has an absorption length

of $\alpha = 17.3$ nm [33] in iron. Thus, if the electrons at the surface reach a temperature in the order of $T_S \approx 1000$ K [32], the electron gas 20 nm deeper is hundreds of degrees colder. The strong electron-electron interaction thermalizes the electron gas efficiently [2, 34], wherefore we describe it by a local Fermi–Dirac distribution $f(T(z))$, see section 3. We assume the pump pulse to be sufficiently short in order to neglect heat transport into the bulk during the action of the pulse. The initial temperature profile of the pumped system is now only a function of the surface temperature and the absorption length α,

$$T(z) = T_S e^{-z/2\alpha}. \tag{3}$$

The factor 1/2 in the exponent accounts for the fact that the internal energy of an electron gas scales quadratic with its temperature. Please note that equation (3) is an approximation based on Beers law. Equation (3) implies that a laser pulse always causes a temperature gradient. Therefore, thermoelectric effects will become important:

In the most general way, the interplay between charge-, spin-, and heat-current densities ($\vec{j}_c$, $\vec{j}_s$, and $\vec{Q}$) can be expressed for a mono-domain, isotropic, and metallic ferromagnet as a matrix equation [35]:

$$\begin{pmatrix} \vec{j}_c \\ \vec{j}_s \\ \vec{Q} \end{pmatrix} = \sigma \begin{pmatrix} 1 & P & ST \\ P & 1 & P'ST \\ ST & P'ST & \kappa T/\sigma \end{pmatrix} \begin{pmatrix} \nabla \mu_c/q \\ \nabla \mu_s/2q \\ -\nabla T/T \end{pmatrix}. \tag{4}$$

Here, $P = (\sigma_\uparrow - \sigma_\downarrow)/\sigma$ is the conductivity spin polarization, $\sigma = \sigma_\uparrow + \sigma_\downarrow$ and $P' = \frac{\partial(P\sigma)/\partial E|_{E_F}}{\partial\sigma/\partial E|_{E_F}}$, κ the thermal conductivity, q the elementary charge, and S the Seebeck coefficient. $\mu_c = \frac{\mu_\uparrow + \mu_\downarrow}{2}$ is the driving potential for the charge current, whereas $\mu_s = \frac{\mu_\uparrow - \mu_\downarrow}{2}$ drives the spin current. The charge current density $\vec{j}_c = 0$ vanishes due to charge neutrality and efficient screening [22] which leads to a spin current density of

$$\vec{j}_s = \sigma\left(\frac{\nabla\mu_s}{2q}(1 - P^2) + (P - P')S\nabla T\right). \tag{5}$$

The last term in equation (5) describes the spin-Seebeck effect. In section 5, we show that the temperature induced shifts of the chemical potentials dominate over the Seebeck effect for high temperatures. However, the Spin-Seebeck effect can be significant at interfaces as well as at lower electron gas temperatures [21, 22, 36]. Neglecting the Seebeck term, equation (5) simplifies to

$$\vec{j}_s = \nabla\mu_s \frac{\sigma}{2q}(1 - P^2). \tag{6}$$

$\vec{j}_s$ is only dependent on the *difference* of the electrochemical potentials, which is equal to the difference of the chemical potentials. Therefore, $\mu_{\uparrow,\downarrow}$ denote the *chemical* potentials for the rest of this manuscript.

In order to estimate the initial spin current density in a laser-induced demagnetization experiment, we assume that the generated temperature profile does not change with time. This decouples the spin current from heat transport. However, this approximation is only valid for the first ≈100 fs [37].

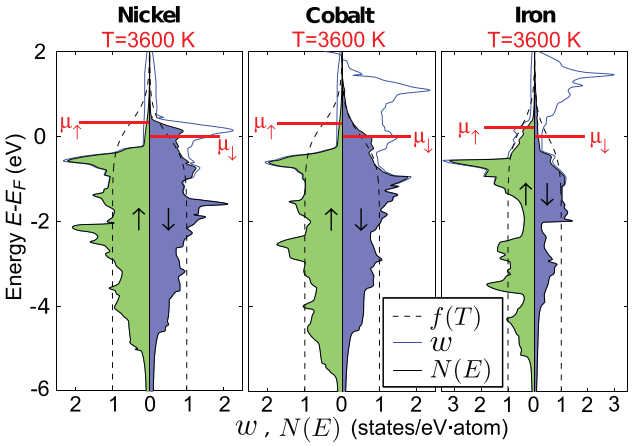

Figure 3. The density of states $w_{\uparrow,\downarrow}$ for majority (↑) and minority (↓) electrons and the corresponding chemical potentials $\mu_{\uparrow,\downarrow}$. $N(E) = w_{\uparrow,\downarrow} f$ represents the density of occupied states at a temperature of $T = 3600$ K, highlighted with different colors for each spin direction. The dashed lines represent the Fermi statistics $f(T)$ for each spin population. The $w_{\uparrow,\downarrow}$ are from [38]. Reproduced with permission from [23].

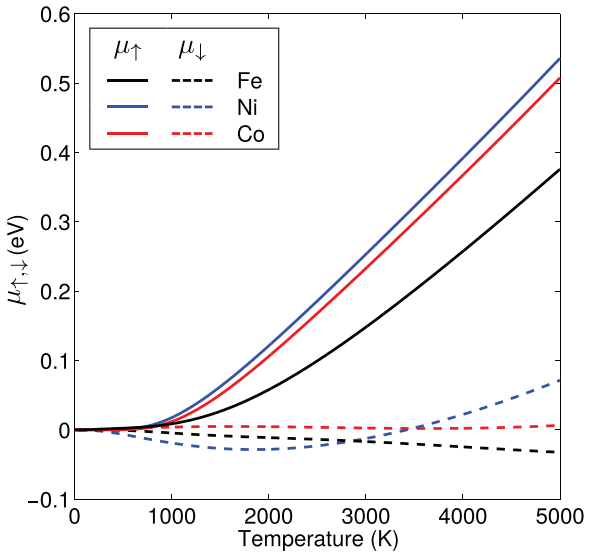

Figure 4. The shifts of the chemical potentials as a function of the temperature for Ni, Fe and Co, calculated by numerically solving equation (7). The dashed lines show the shifts of the majority chemical potentials $\mu_\downarrow$ whereas the solid lines show the shifts of $\mu_\uparrow$. The colors indicate the elements Fe (black), Ni (blue) and Co (red). The density of states was taken from [38]. Reproduced with permission from [23].

We focus on the case of iron, but the arguments can likewise be used for the other transition metal ferromagnets nickel and cobalt. The large electron temperature at the surface causes a local change of the chemical potentials $\mu_{\uparrow,\downarrow}(T)$ for minority and majority electrons, respectively. The chemical potentials are acquired by numerically solving the implicit equations for the density of majority ($n_\uparrow$) and minority ($n_\downarrow$) electrons

$$n_{\uparrow,\downarrow}(T = 0\,\mathrm{K}, \mu_{\uparrow,\downarrow} = E_f) = n_{\uparrow,\downarrow}(T, \mu_{\uparrow,\downarrow}(T)). \tag{7}$$

For the validity of these equations, we neglect spin flips during the heating pulse. In addition, we rely on strong electron-electron interaction to equilibrate the temperatures of the minority

Table 1. Compilation of literature data for figure 1. Reproduced with permission from [23].

Sample	d (nm)	τ (fs)	T (K)	ρ ($\mu\Omega$ cm)	On insulator
Gd	10	760 ± 250 [46]	140	66 ± 0.7 [50]	No
Tb	10	740 ± 250 [46]	140	64.5 ± 0.6 [51]	No
Fe	10	98 ± 26 [52]	293	9.61 [42]	No
Fe	7	66 ± 7 [48]	298	9.87 [42]	Yes
Ni	15	177 ± 16 [2]	298	7.12 [42]	No
Ni	10	157 ± 9 [52]	293	6.93 [42]	No
Ni	2.5	25 ± 25 [53]	323	8.26 ± 0.1 [42]	No
Ni	15	120 ± 70 [8]	298	7.12 [42]	No
Ni	10	150 [54]	298	7.12 [42]	No
Ni	17	130 ± 40 [55]	298	7.12 [42]	No
Ni	35	250 ± 100 [56]	298	7.12 [42]	No
Ni	15	184 ± 20 [57]	298	7.12 [42]	No
Ni	20	155 ± 19 [17]	298	7.12 [42]	No
Ni	10	121 ± 44 [58]	293	6.93 [42]	No
Ni	7.5	77 ± 26 [59]	298	7.12 [42]	Yes
Ni	10	74 ± 4 [49]	298	7.12 [42]	Yes
Co	15	199 ± 16 [2]	298	6 ± 0.1 [60]	Yes
Co	0.8	25 ± 25 [53]	323	6.81 [60]	No
$Fe_{80}Ni_{20}$	10	89 ± 8 [52]	293	14 ± 1 [61]	No
$Fe_{80}Ni_{20}$	12	176 ± 12 [62]	298	14 ± 1 [61]	No
CrO_2	—	84 000 [63]	298	250 ± 5 [64]	—
$La_{0.66}Sr_{0.33}MnO_3$	55	$525\,000 \pm 125\,000$ [57]	298	1000 [57]	Yes
Sr_2FeMoO_6	Bulk	$95\,000 \pm 85\,000$ [57]	300	350 ± 20 [65]	Yes
$SrRuO_3$	600	9000 ± 6000 [57]	140	135 ± 10 [66]	No
Fe_3O_4	15	$>10^6$ [57]	298	5000 ± 500 [67]	Yes
CoMnSb	100	18 000 [63]	298	170 ± 10 [68]	No
Co_2MnSi	15	297 [63]	298	19 ± 1 [69]	No

and majority electrons. Notice, that there can be a temperature difference between the two spin populations at the interface to the substrate [22], which is neglected in our model. The electron densities are:

$$n_{\uparrow,\downarrow}(T) = \int_{-\infty}^{\infty} f(T, E, \mu_{\uparrow,\downarrow}(T)) w_{\uparrow,\downarrow}(E) \mathrm{d}E. \tag{8}$$

Here, $w_{\uparrow,\downarrow}(E)$ are the spin dependent densities of states, which are assumed to remain unaffected by the rise in temperature and f being the Fermi–Dirac function.

Figure 3 shows the computed chemical potentials for the Fe, Ni and Co band structure. At zero temperature, the Fermi energy E_F is equal to the chemical potentials for both spins, $\mu_\uparrow = \mu_\downarrow = E_F$. At non-zero temperatures, the chemical potential of the majority and minority electrons *deviate* from the Fermi energy. Figure 4 shows the temperature-induced shifts of the chemical potentials as a function of the temperature for Ni, Fe and Co. The chemical potentials for the majority electrons (solid lines) dominate over the shifts of the minority electrons (dashed lines).

The laser-induced temperature gradient therefore causes a gradient in the chemical potentials along the z-direction. Thus, we have all the ingredients to calculate the initial spin current based on equation (6). If the thickness d of the ferromagnet is smaller than the penetration length of the pump light, we can approximate equation (6) to

$$j_s = \frac{\sigma}{2q}(1 - P^2)(\mu_\uparrow(0) - \mu_\downarrow(0) - \mu_\downarrow(d) + \mu_\uparrow(d)). \tag{9}$$

5. Comparison with experimental evidence

For an iron film of 10 nm thickness and an absorbed pulse energy of 1.3 mJ cm^{-2}, we obtain a surface temperature of approx. 2000 K. According to equation (3), the temperature at the interface to the substrate is 1500 K. This leads to a shift of the chemical potentials of $\mu_\uparrow(z = 0) - \mu_\uparrow(z = d) = 30$ meV and $\mu_\downarrow(z = 0) - \mu_\downarrow(z = d) \approx 0$ meV. In comparison, we estimate the Seebeck term as follows: Hatami *et al* [39] calculate P' for various magnetic interfaces. Typical values for $|P'|$ are below 2. The Seebeck coefficient of Fe is 0.4 μV K^{-1} at 1000 K [40]. The spin voltage generated by the Seebeck effect is

$$U_s = \int_0^d S(P - P')\nabla T \mathrm{d}z \approx S(P - P')\Delta T \tag{10}$$

which is on the order of 0.5 mV. However, if the temperatures are lower, the Seebeck term can be larger: $S(300\ \mathrm{K}) = 14\ \mu\mathrm{V\ K^{-1}}$

[40]. In addition, the chemical potential shifts are significantly smaller, as shown in figure 4. Therefore, the Seebeck term will dominate the spin current generation at low temperatures.

The majority conductivity is larger than the minority conductivity as $\sigma_\downarrow \approx \frac{1}{4}\sigma_\uparrow$ [41] with $\sigma = 1.0 \cdot 10^7$ A Vm^{-1} [42]. For iron, we obtain a spin current density of 10^9 A cm^{-2}.

The most direct measurement of the spin current has been performed by Kampfrath *et al* [18]. Here, the spin current generated by the ferromagnet is measured by taking advantage of the spin-Hall effect: the spin current is injected into a gold film, where it is transformed into a lateral charge current pulse. The current pulse causes the emission of electromagnetic radiation in the THz range. The THz field is measured and used to determine the temporal evolution of the spin current. Kampfrath *et al* detected a maximum spin current density of $1.3 \cdot 10^9$ A cm^{-2}, which is reached approx. 50 fs after the laser pulse. Our simple thermodynamic model is in good agreement with this measurement.

Other groups have used a different approach to measure the laser-induced spin current: they inject the spin current into a second ferromagnet with magnetization $\vec{M}_2$. There, the spin torque changes $\vec{M}_2$. If the injected spin direction is parallel or anti-parallel to the magnetization $|\vec{M}_2|$ is altered [19]. If there is an angle between $\vec{M}_2$ and the spin direction, the magnetization starts to precess [36, 43].

These spin injection experiments are conceptually similar to current induced switching in giant magnetic resistance nanopillars [30]. However, the pure spin current generated by the laser-excited ferromagnet does not generate an Oersted field, which simplifies the dynamics [44]. In addition, the time structure of the laser generated spin current pulses reaches the femtosecond time scale, which is not achievable for electrically driven devices.

6. The role of the interface for the demagnetization

The transport of the spin current from the ferromagnet to the substrate requires passing the interface. However, the interface may not be transparent for the spin current. As indicated in section 2, the spin current can change along its path of transport due to spin flips. Some spin flips occur in the bulk of the ferromagnet and the substrate. The interface itself can also act as a very effective, localized spin flip scatterer. The reason is that the symmetry is broken along z, leading to an enhanced spin-orbit coupling. The spin-orbit coupling is the root cause for transferring angular momentum from the spin system to the lattice. One indication of this effect has been found by Erekhinsky *et al* [45] in a transport experiment. Another indication is the fact, that for gadolinium, the surface demagnetizes within $<$100 fs (measured by second harmonic magneto-optical Kerr effect [46]), whereas the bulk needs approx. 1 ps [47]. This effect may strengthen the contribution of transport for ultrafast demagnetization. This is even the case on insulating substrates [48, 49]: here, the interface can act as a spin flip scatterer, although there is no spin current present in the substrate.

7. Conclusions

The generation of spin currents caused by ultrafast demagnetization has been proposed theoretically by Battiato *et al* [15]. Their model is based on a Monte-Carlo simulation of individual electrons flowing in a super-diffusive manner. Here, we have presented an easily understandable thermodynamic model capable of describing the magnitude of spin currents in a purely diffusive manner. The absorbed pump laser light causes a temperature gradient of the electron gas. In the framework of thermodynamics, we can estimate the shift of the chemical potentials due to the increased temperature. As the density of states is spin split, the chemical potential shifts are spin dependent. The gradient of these potentials are the driving forces for a spin current. The magnitude of the spin current is in agreement with experimental data from other groups. The spin currents are not only a relevant contribution for ultrafast demagnetization, but can also be utilized to bring the femtosecond time scale to the field of spintronics.

Acknowledgments

We thank A Vindigni, C Stamm, K Bühlmann, D Pescia, and M Battiato for the very fruitful discussions. This work was supported by the Swiss National Science Foundation and by ETH Zurich. A Fognini greatly acknowledges support by the Swiss National Science Foundation's Early Postdoc Mobility program.

References

[1] Beaurepaire E, Merle J C, Daunois A and Bigot J Y 1996 *Phys. Rev. Lett.* **76** 4250
[2] Koopmans B, Malinowski G, Longa F D, Steiauf D, Fähnle M, Roth T, Cinchetti M and Aeschlimann M 2010 *Nat. Mater.* **9** 259
[3] Schmidt A B, Pickel M, Donath M, Buczek P, Ernst A, Zhukov V P, Echenique P M, Sandratskii L M, Chulkov E V and Weinelt M 2010 *Phys. Rev. Lett.* **105** 197401
[4] Krauß M, Roth T, Alebrand S, Steil D, Cinchetti M, Aeschlimann M and Schneider H C 2009 *Phys. Rev.* B **80** 180407
[5] Steiauf D and Fähnle M 2009 *Phys. Rev.* B **79** 140401
[6] Carva K, Battiato M and Oppeneer P M 2011 *Phys. Rev. Lett.* **107** 207201
[7] Zhang G P, Hübner W, Lefkidis G, Bai Y and George T F 2011 *Nat. Phys.* **7** 665
[8] Stamm C *et al* 2007 *Nat. Mater.* **6** 740
[9] Zhang G P and Hübner W 2000 *Phys. Rev. Lett.* **85** 3025
[10] Fabian J and Das Sarma S 1998 *Phys. Rev. Lett.* **81** 5624
[11] Steiauf D, Illg C and Fähnle M 2010 *J. Magn. Magn. Mater.* **322** L5
[12] Töws W and Pastor G M 2015 *Phys. Rev. Lett.* **115** 217204
[13] Roth T, Schellekens A J, Alebrand S, Schmitt O, Steil D, Koopmans B, Cinchetti M and Aeschlimann M 2012 *Phys. Rev.* X **2** 021006
[14] Mueller B Y, Roth T, Cinchetti M, Aeschlimann M and Rethfeld B 2011 *New J. Phys.* **13** 123010
[15] Battiato M, Carva K and Oppeneer P M 2010 *Phys. Rev. Lett.* **105** 027203

[16] Malinowski G, Longa F D, Rietjens J H H, Paluskar P V, Huijink R, Swagten H J M and Koopmans B 2008 *Nat. Phys.* **4** 855
[17] Eschenlohr A, Battiato M, Maldonado P, Pontius N, Kachel T, Holldack K, Mitzner R, Föhlisch A, Oppeneer P M and Stamm C 2013 *Nat. Mater.* **12** 332
[18] Kampfrath T *et al* 2013 *Nat. Nanotechnol.* **8** 256
[19] Rudolf D *et al* 2012 *Nat. Commun.* **3** 1037
[20] Turgut E *et al* 2013 *Phys. Rev. Lett.* **110** 197201
[21] Kimling J, Choi G M, Brangham J T, Matalla-Wagner T, Huebner T, Kuschel T, Yang F and Cahill D G 2017 *Phys. Rev. Lett.* **118** 057201
[22] Kimling J and Cahill D G 2017 *Phys. Rev.* B **95** 014402
[23] Fognini A 2014 Ultrafast demagnetization: an electronic point of view *PhD Thesis ETH* Zurich (https://doi.org/10.3929/ethz-a-010192516)
[24] Stöhr J and Siegmann H 2006 *Magnetism, From Fundamentals to Nanoscale Dynamics* (New York: Springer) (https://doi.org/10.1007/978-3-540-30283-4)
[25] Jedema F J, Filip A T and van Wees B J 2001 *Nature* **410** 345
[26] Hirsch J E 1999 *Phys. Rev. Lett.* **83** 1834
[27] Valet T and Fert A 1993 *Phys. Rev.* B **48** 7099
[28] Binasch G, Grünberg P, Saurenbach F and Zinn W 1989 *Phys. Rev.* B **39** 4828
[29] Baibich M N, Broto J M, Fert A, Van Dau F N, Petroff F, Etienne P, Creuzet G, Friederich A and Chazelas J 1988 *Phys. Rev. Lett.* **61** 2472
[30] Katine J A, Albert F J, Buhrman R A, Myers E B and Ralph D C 2000 *Phys. Rev. Lett.* **84** 3149
[31] Kiselev S I, Sankey J C, Krivorotov I N, Emley N C, Schoelkopf R J, Buhrman R A and Ralph D C 2003 *Nature* **425** 380
[32] Rhie H S, Dürr H A and Eberhardt W 2003 *Phys. Rev. Lett.* **90** 247201
[33] Weaver J H and Frederikse H P R 2011–2012 Chapter: Optical properties of selected elements *Handbook of Chemistry and Physics* 92nd edn (Boca Raton, FL: CRC Press)
[34] Dürr H 2009 *Nucl. Instrum.* A **601** 132
[35] Bauer G E W, Saitoh E and van Wees B J 2012 *Nat. Mater.* **11** 391
[36] Choi G M, Min B C, Lee K J and Cahill D G 2014 *Nat. Commun.* **5** 4334
[37] Salvatella G, Gort R, Bühlmann K, Däster S, Vaterlaus A and Acremann Y 2016 *Struct. Dyn.* **3** 055101
[38] Moruzzi V L, Janak J F and Williams A R 1978 *Calculated Electronic Properties of Metals* (New York: Pergamon)
[39] Hatami M, Bauer G E W, Zhang Q and Kelly P J 2007 *Phys. Rev. Lett.* **99** 066603
[40] Berger L 2017 Chapter: Thermal emf (Seebeck coefficient) of elemental metals *CRC Handbook of Chemistry and Physics* 97th edn, ed W Haynes (Boca Raton, FL: CRC Press) (Internet version)
[41] Fert A and Campbell I A 1976 *J. Phys. F: Met. Phys.* **6** 849
[42] Haynes W M (ed) 2012 Chapter: Electrical resistivity of pure metals *CRC Handbook of Chemistry and Physics* 93rd edn (London: Taylor & Francis)
[43] Schellekens A J, Kuiper K C, de Wit R R J C and Koopmans B 2014 *Nat. Commun.* **5** 4333
[44] Strachan J P *et al* 2008 *Phys. Rev. Lett.* **100** 247201
[45] Erekhinsky M, Sharoni A, Casanova F and Schuller I 2010 *Appl. Phys. Lett.* **96** 022513
[46] Wietstruk M, Melnikov A, Stamm C, Kachel T, Pontius N, Sultan M, Gahl C, Weinelt M, Dürr H A and Bovensiepen U 2011 *Phys. Rev. Lett.* **106** 127401
[47] Lisowski M, Loukakos P A, Melnikov A, Radu I, Ungureanu L, Wolf M and Bovensiepen U 2005 *Phys. Rev. Lett.* **95** 137402
[48] Carpene E, Mancini E, Dallera C, Brenna M, Puppin E and De Silvestri S 2008 *Phys. Rev.* B **78** 174422
[49] Longa F D, Kohlhepp J T, de Jonge W J M and Koopmans B 2007 *Phys. Rev.* B **75** 224431
[50] Colvin R V and Arajs S 1964 *Phys. Status Solidi* B **4** 37
[51] Arajs S and Colvin R V 1964 *Phys. Rev.* **136** A439
[52] Mathias S *et al* 2012 *Proc. Natl Acad. Sci.* **109** 4792
[53] Güdde J, Conrad U, Jähnke V, Hohlfeld J and Matthias E 1999 *Phys. Rev.* B **59** R6608
[54] Koopmans B, Ruigrok J J M, Longa F D and de Jonge W J M 2005 *Phys. Rev. Lett.* **95** 267207
[55] Stamm C, Pontius N, Kachel T, Wietstruk M and Dürr H A 2010 *Phys. Rev.* B **81** 104425
[56] Kachel T, Pontius N, Stamm C, Wietstruk M, Aziz E F, Dürr H A, Eberhardt W and de Groot F M F 2009 *Phys. Rev.* B **80** 092404
[57] Müller G M *et al* 2009 *Nat. Mater.* **8** 56
[58] La-O-Vorakiat C *et al* 2012 *Phys. Rev.* X **2** 011005
[59] Bigot J Y, Vomir M and Beaurepaire E 2009 *Nat. Phys.* **5** 515
[60] Bass J 1983 Chapter: Co–Hf, pure metal resistivities from $T = 10$–15 K till melting point *Springer Materials—The Landolt-Börnstein Database* (https://doi.org/10.1007/10307022_5)
[61] Mayadas A F, Janak J F and Gangulee A 1974 *J. Appl. Phys.* **45** 2780
[62] Walowski J, Müller G, Djordjevic M, Münzenberg M, Kläui M, Vaz C A F and Bland J A C 2008 *Phys. Rev. Lett.* **101** 237401
[63] Mann A *et al* 2012 *Phys. Rev.* X **2** 041008
[64] Lewis S P, Allen P B and Sasaki T 1997 *Phys. Rev.* B **55** 10253
[65] Yanagihara H, Cheong W, Salamon M B, Xu S and Moritomo Y 2002 *Phys. Rev.* B **65** 092411
[66] Klein L, Dodge J S, Ahn C H, Snyder G J, Geballe T H, Beasley M R and Kapitulnik A 1996 *Phys. Rev. Lett.* **77** 2774
[67] Ziese M and Blythe H J 2000 *J. Phys.: Condens. Matter.* **12** 13
[68] Otto M J, van Woerden R A M, van der Valk P J, Wijngaard J, van Bruggen C F and Haas C 1989 *J. Phys.: Condens. Matter.* **1** 2351
[69] Ritchie L, Xiao G, Ji Y, Chen T Y, Chien C L, Zhang M, Chen J, Liu Z, Wu G and Zhang X X 2003 *Phys. Rev.* B **68** 104430